

Chapter 5

Circular Discs Squeeze-Film Bearings with Porous Roughness Effects at the Lower Disc

Contents

5.1 Introduction

5.2 Formulation of the Mathematical Model

5.2.1 Distribution of Roughness Heights

5.3 Solution

5.4 Results and Discussion

5.5 Conclusions

5.6 Figures

5.7 References

5.1 Introduction

In recent years, many theoretical and experimental inventions are made on the bearing design systems as well as lubricating substances in order to increase the efficiency of the bearing performances. One major revolution in the direction of lubricating substances is an invention of Ferrofluids. Ferrofluids (FFs) or Magnetic fluids (MFs) [1] are stable colloidal suspensions containing fine ferromagnetic particles dispersing in a liquid, called carrier liquid, in which a surfactant is added to generate a coating layer preventing the flocculation of the particles. When an external magnetic field \mathbf{H} is applied, FFs experience magnetic body force $(\mathbf{M} \cdot \nabla)\mathbf{H}$ which depends upon the magnetization vector \mathbf{M} of ferromagnetic particles and are oriented along the field lines. The main property of FFs is that they can be made to adhere to any preferred place with the help of magnets and to move even in zero gravity regions. Due to these features, FFs are used in many applications including lubrication of bearing design systems [2,3]. Recently, many theoretical investigations are made using FFs as lubricant owing to its various advantages such as long life, silent operation and reduction of wear. As the present Chapter deals with the study of FF lubricated squeeze-film-bearings with porous-roughness effect, the following are some references regarding squeeze-film-bearings discussed by different authors from different viewpoints. It should be noted that squeeze-film arise when two lubricated surfaces (discs or plates) approaches each other with a normal velocity (known as squeeze velocity). Squeeze-film characteristics plays an important role in many applications, namely, lubrication of machine elements, artificial joints, etc.

Starting with 1974, Murti [4] discussed porous circular discs squeeze-film-bearing, where the porous layer is attached with the upper impermeable disc. Three bearing characteristics like pressure distribution, load-carrying capacity and response time are discussed in terms of Fourier-Bessel series. It is found that an enhanced value for the permeability parameter diminishes the pressure over the entire disc and also evens out the pressure distribution; however, there is an adverse effect on the load-carrying capacity and response time of approach. The porous effects are shown to predominate at very low thickness values. Ting [5] analyzed lubricated clutch engagement behaviour of two annular discs with the elastically deformable porous facing attached with the above disc. The surface roughness is also introduced at both the discs. The bearing characteristics like pressure distribution, load-carrying capacity and film thickness versus time have been studied. Prakash and Tonder [6] describe a theoretical analysis of the effects of surface roughness on squeeze-film characteristics between two circular plates. It is found that the circumferential roughness reduces the sinkage rate of the squeeze plate. If the highest asperities are blunt or flat, the theoretical time to reach the rest position may tend to infinity. In the case of radial roughness, the sinkage rate is increased. Verma [7] discussed squeeze-film between two rectangular plates using MF lubricant. The upper surface is a rigid rectangular smooth plate while the lower one is composed of three thin porous layers with different porosities. Explicit solutions for the velocity, pressure and the load-carrying capacity are obtained. It is found that the time for the upper plate to come down is longer than viscous squeeze-film. Thus, better performance of the MF effect is observed. Bhat and Deheri [8] theoretical studied the squeeze-film between two circular discs, where the porous layer is attached with the upper disc. It is found that pressure, load capacity and

response time are increased with the increasing values of magnetization of MF. The effects due to magnetization are found to be independent of the curvature of the upper disc. Elsharkawy and Nassar [9] found closed form of analytical solutions for three different types (parallel surface bearing of infinite width, journal bearing and parallel circular plates) of squeeze-film porous bearings. The results show that as the permeability parameter increases, both the pressure profiles and the load-carrying capacity decreases. It is also shown that the effect of the porous layer can be neglected when dimensionless permeability parameter less than 0.001. Shah *et. al.* [10] theoretically analyzed squeeze-film behaviour between rotating annular plates, where the upper exponentially curved plate is attached with a porous facing of uniform thickness while the lower one is impermeable flat. The lubricant used is MF, which is controlled by oblique magnetic field. The results show that the increase in pressure and load-carrying capacity depended only on the magnetization while increase in response time depended on magnetization, fluid inertia and speed of rotation of the plates. Usha and Vimala [11] theoretically predicted the squeeze-film force in a circular Newtonian squeeze-film using the elliptical velocity profile assumption by three different approximation methods – momentum integral method, successive approximation method and energy integral method. The results show good agreement with the experimental test. Shah and Bhat [12] analyzed FF squeeze-film in an axially undefined porous journal bearing considering anisotropic permeability of the porous facing and slip velocity at the film-porous interface. The results show that load-carrying capacity and response time increases with the increasing values of eccentricity ratio and anisotropic parameter, while they decreased with the increasing values of slip parameter or material parameter. Jaffar [13] studied squeeze-films between a rigid

cylinder and an elastic layer bonded to a rigid foundation. Influences of the layer thickness, the layer compressibility and the central squeeze-film velocity on the results are investigated. Bujurke *et. al.* [14] studied surface roughness effects on the squeeze-film between circular upper porous-rough surface and lower solid rough surface using couple stress fluid. The results show that effects of couple stress fluid and surface roughness is more pronounced compared to classical case. Rajashekar and Kashinath [15] analyzed combined effects of couple stress and surface roughness on MHD squeeze-film lubrication between a sphere and a porous-rough plane. The results show that the couple stress fluid enhances the mean pressure, load-carrying capacity and squeeze-film time. Also, the effects of roughness parameter increase (decrease) the load-carrying capacity and lengthen the response time for azimuthal (radial) roughness patterns as compared to the smooth case. The effect of porous parameter decrease the load-carrying capacity and increase the squeeze-film time as compared to the solid case. Kesavan *et. al.* [16] analyzed the surface roughness effect on the squeeze-film characteristics between finite porous parallel rectangular plates lubricated with an electrically conducting fluid in the presence of a transverse magnetic field. It is found that load-carrying capacity and response time increases with the increase of magnetic field effect. Walicka *et. al.* [17] discussed effects of bearing surfaces and porosity of one bearing surface on pressure distribution and load-carrying capacity using bingham fluid. The general formulae for pressure and load-carrying capacity are derived. Fathima *et. al.* [18] studied performance of hydromagnetic squeeze-film between anisotropic porous rectangular plates with couple stress fluids. Here, the magnetic field considered is transverse. The results show the increase in load-carrying capacity and lengthen the squeeze time as compared to nonmagnetic case. Lin *et.*

al. [19] investigated effects of circumferential and radial rough surfaces in a non-Newtonian MF lubricated circular squeeze-film. Here, both the discs are solid impermeable. The results show that the circumferential roughness effect increases the mean load capacity and lengthen the mean approaching time as compared to those of smooth discs. However, the radial roughness patterns yield a reverse trend. Shah *et. al.* [20-22] studied FF based squeeze-films between sphere and flat porous plate, rotating sphere and radially rough plate and some reviews on squeeze-films, respectively. Everywhere better performances of the squeeze-film characteristics are indicated.

The aim of the present Chapter is to study the circular squeeze-film-bearing phenomenon formed between upper solid impermeable disc and lower porous-rough disc with the effects of two roughness patterns (radial and circumferential) on the porous surface using FF lubricant. Here, the FF is controlled by oblique radially variable magnetic field (VMF) because of obtaining advantage of generating maximum field at the required active contact zone. Moreover, the VMF is considered because uniform magnetic field does not enhance bearing performances. The porous-rough surface is considered because of obtaining advantage of self-lubricating property. Using FF flow model by R. E. Rosensweig and roughness effect by Christensen's stochastic theory modified Reynolds equation is derived, which is solved for load-carrying capacity for different shapes (exponential, secant, mirror image of secant and parallel) of the upper disc. The results are compared among different shapes and the impacts of permeability and roughness patterns are studied. The purpose of considering the present problem is lies in the observation that the studies of most of different designs squeeze-films (sphere-plate, cylindrical-disc, two-

parallel plates, etc.) reduce to the present case or present case is the limiting case of different designs squeeze-films.

5.2 Formulation of the Mathematical Model

Figure 5.1 shows the configuration of the present circular squeeze-film-bearing design, where the upper disc is solid impermeable while the lower one is porous-rough. Both the discs are having radius a . The porous-rough disc is made by attaching a porous facing (region or matrix) of thickness (or width) H^* with the solid impermeable disc. Practically the porous facing is rough, so two roughness patterns (radial and circumferential) are considered for the study. The gap between two discs (known as film region) is filled with FF, which leads FF film and may be of different shapes due to the different designs (exponential, secant, mirror image of secant and parallel) of the upper disc. The upper disc rotate with an angular (or rotational) velocity Ω_u while the lower with Ω_l . The upper disc moves normally towards lower one with a normal velocity (known as squeeze velocity)

$$\dot{h}_0 = \frac{dh_0}{dt}, \quad (5.1)$$

where h_0 is the central film thickness at time $t = 0$.

Also,

$$\mathbf{q} = (\dot{r}, r\dot{\theta}, \dot{z}) = (u, rv, w). \quad (5.2)$$

Here, (r, θ, z) are cylindrical polar co-ordinates and dot ($\dot{\cdot}$) represents derivative w.r.t. t .

In the present case, the strength of the oblique radially VMF, which controls FF in the film region, can be considered as

$$H^2 = \frac{Kr^2(a-r)}{a}, \quad (5.3)$$

in order to get maximum field strength at $r = 2a / 3$. This strength can be considered because, in the present case, neighbourhood of $r = 2a / 3$ is active contact zone. For other active contact zones, different forms of magnetic field should be chosen. Here, r is the radial co-ordinate and K being a quantity chosen to suit the dimensions of both sides of equation (5.3).

For an incompressible, steady, axisymmetric flow, equations (2.25) to (2.29) in cylindrical polar co-ordinates in r (radial)-direction (referring [21]) becomes

$$-\frac{v^2}{r} = -\frac{1}{\rho} \frac{\partial}{\partial r} \left(p - \frac{1}{2} \mu_0 \bar{\mu} H^2 \right) + \frac{\eta}{\rho} \frac{\partial^2 u}{\partial z^2} \quad (5.4)$$

under the usual assumptions of lubrication, neglecting inertia terms and that the derivatives of fluid velocities across the film predominate. Here, z is axial co-ordinate.

By considering tangential component v of velocity vector \mathbf{q} of both the discs [10,21], equation (5.4) becomes

$$\frac{\partial^2 u}{\partial z^2} = \frac{1}{\eta} \left[\frac{\partial}{\partial r} \left(p - \frac{1}{2} \mu_0 \bar{\mu} H^2 \right) - \rho r \left(\frac{z}{h} \Omega_r + \Omega_l \right)^2 \right]; \quad \Omega_r = \Omega_u - \Omega_l, \quad (5.5)$$

where h is the film thickness made up of two parts

$$h = h_n(r) + h_s(r, \theta, \xi); \quad (5.6)$$

h_n denotes the nominal smooth part of the film geometry and h_s is the part due to the surface asperities measured from nominal level and is a randomly varying quantity with zero mean, ξ being an index determining a definite roughness arrangement.

Using boundary conditions [20]

$$u = \frac{1}{s} \frac{\partial u}{\partial z} \quad \text{when } z = 0 ; \quad \frac{1}{s} = \frac{\sqrt{\phi_r \eta_r}}{5} \quad (\text{Slip condition})$$

and

$$u = 0 \quad \text{when } z = h \quad (\text{No slip condition}),$$

equation (5.5) yields velocity profile in the film region as

$$\begin{aligned} u = \frac{1}{\eta(1+sh)} & \left[\frac{(z-h)(z+h+szh)}{2} \frac{\partial}{\partial r} \left(p - \frac{1}{2} \mu_0 \bar{\mu} H^2 \right) \right. \\ & + \frac{\rho r \Omega_r^2}{12 h^2} (-z^4 + h^4 - sz^4 h + szh^4) \\ & + \frac{\rho r \Omega_r \Omega_l}{3 h} (-z^3 + h^3 + szh^3 - sz^3 h) \\ & \left. + \frac{\rho r \Omega_l^2}{2} (-z^2 - sz^2 h + szh^2 + h^2) \right], \end{aligned} \quad (5.7)$$

where s is a slip parameter, ϕ_r being the permeability of FF in the porous matrix in the radial direction and η_r being the porosity in the same direction.

Substituting u from equation (5.7) in the cylindrical polar form of continuity equation (2.26) for film region, and integrating it over the film thickness $(0, h)$, the transverse velocity component w at $z = 0$ emerges in the form

$$w_0 = \frac{1}{r} \frac{\partial}{\partial r} \left[\left\{ -\frac{r(4h^3 + sh^4)}{12\eta(1+sh)} \frac{\partial}{\partial r} \left(p - \frac{1}{2} \mu_0 \bar{\mu} H^2 \right) \right\} + \frac{\rho r^2}{120\eta(1+sh)} \left\{ \begin{aligned} & sh^4(3\Omega_u^2 + 4\Omega_u \Omega_l + 3\Omega_l^2) \\ & + 2h^3(4\Omega_u^2 + 7\Omega_u \Omega_l + 9\Omega_l^2) \end{aligned} \right\} \right] - \dot{h}_0, \quad (5.8)$$

where $w_h = -\dot{h}_0$, squeeze velocity.

Assuming the validity of the Darcy's law and considering the contributions from magnetic pressure and rotation, the radial and axial components of the fluid velocity in the porous matrix are given by [23]

$$\bar{u} = -\frac{\phi_r}{\eta} \left[\frac{\partial}{\partial r} \left(P - \frac{1}{2} \mu_0 \bar{\mu} H^2 \right) - \rho r \Omega_l^2 \right] \text{ (} r \text{- direction),}$$

(5.9)

$$\bar{w} = -\frac{\phi_z}{\eta} \left[\frac{\partial}{\partial z} \left(P - \frac{1}{2} \mu_0 \bar{\mu} H^2 \right) \right] \text{ (} z \text{- direction),}$$

(5.10)

where ϕ_z is the permeability of FF in the porous matrix in the axial direction and P is the fluid pressure there.

Substituting these \bar{u} and \bar{w} in the cylindrical polar form of continuity equation (2.26) for the porous matrix and integrating it over the width of the porous matrix ($-H^*$, 0), yields

$$\bar{w}_0 = \frac{1}{r} \frac{\partial}{\partial r} \left[\frac{\phi_r H^*}{\eta} r \frac{\partial}{\partial r} \left(P - \frac{1}{2} \mu_0 \bar{\mu} H^2 \right) \right] - \frac{2\rho \phi_r H^* \Omega_l^2}{\eta}$$

(5.11)

using Morgan-Cameron approximation [24] and the fact that the surface $z = -H^*$ is impermeable.

By assuming the continuity of the normal (axial) component of the fluid velocity at the film-porous interface at the lower disc; that is,

$$w_0 = \bar{w}_0$$

yields

$$\begin{aligned}
& \frac{1}{r} \frac{\partial}{\partial r} \left[\left(12\phi_r H^* + \frac{4h^3 + sh^4}{1+sh} \right) r \frac{\partial}{\partial r} \left(p - \frac{1}{2} \mu_0 \bar{\mu} H^2 \right) \right] \\
& = \frac{1}{r} \frac{\partial}{\partial r} \left[\frac{\rho r^2}{10(1+sh)} \left\{ sh^4 (3\Omega_u^2 + 4\Omega_u \Omega_l + 3\Omega_l^2) \right. \right. \\
& \quad \left. \left. + 2h^3 (4\Omega_u^2 + 7\Omega_u \Omega_l + 9\Omega_l^2) \right\} \right] - 12\eta \dot{h}_0 + 24\rho \phi_r H^* \Omega_l^2
\end{aligned} \tag{5.12}$$

using equations (5.8)-(5.11).

5.2.1 Distribution of Roughness Heights

With film thickness being regarded as a random quantity because of roughness effect, a height distribution function must be associated. Therefore, a polynomial form, approximating the Gaussian is chosen. Such a probability density function of the stochastic film thickness, h_s , is taken as [6,25]

$$f(h_s) = \begin{cases} \frac{35}{32c^7} (c^2 - h_s^2)^3; & -c < h_s < c \\ 0 & ; \text{ elsewhere} \end{cases}, \tag{5.13}$$

where $c = \pm 3\sigma$, and σ is the standard deviation.

In the context of stochastic theory [6,25], the analysis is usually done for two types of one-dimensional roughness patterns (viz. radial and circumferential) as follows.

Radial Roughness Pattern

In this model, the roughness is assumed to have the form of long, narrow ridges and valleys running in r -direction (that is, they are straight ridges and valleys passing through $z = 0$, $r = 0$ to form a star pattern). The film thickness in this case assumes the form

$$h = h_n + h_s(\theta, \xi). \quad (5.14)$$

Taking expected values of both sides of equation (5.12), yields (referring [26])

$$\begin{aligned} & \frac{1}{r} \frac{\partial}{\partial r} \left[\left\{ 12\phi_r H^* + \frac{4E(h^3) + sE(h^4)}{1 + sE(h)} \right\} r \frac{\partial}{\partial r} \left\{ E(p) - \frac{1}{2} \mu_0 \bar{\mu} H^2 \right\} \right] \\ &= \frac{1}{r} \frac{\partial}{\partial r} \left[\frac{\rho r^2}{10\{1 + sE(h)\}} \left\{ \begin{aligned} & s E(h^4)(3\Omega_u^2 + 4\Omega_u\Omega_l + 3\Omega_l^2) \\ & + 2 E(h^3)(4\Omega_u^2 + 7\Omega_u\Omega_l + 9\Omega_l^2) \end{aligned} \right\} \right] - 12\eta \dot{h}_0 + 24\rho\phi_r H^* \Omega_l^2, \end{aligned} \quad (5.15)$$

where $E(*)$ is the expectancy operator defined by

$$E(*) = \int_{-\infty}^{\infty} (*) f(h_s) dh_s; \quad (5.16)$$

$f(h_s)$ is defined in equation (5.13).

Using equation (5.16) stochastic Reynolds equation in this case can be obtained as

$$\begin{aligned} & \frac{1}{r} \frac{\partial}{\partial r} \left[\left\{ 12\phi_r H^* + \frac{4 \left(h_n^3 + \frac{c^2}{3} h_n \right) + s \left(h_n^4 + \frac{2c^2}{3} h_n^2 + \frac{c^4}{33} \right)}{1 + s h_n} \right\} r \frac{\partial}{\partial r} \left\{ E(p) - \frac{1}{2} \mu_0 \bar{\mu} H^2 \right\} \right] \\ &= \frac{1}{r} \frac{\partial}{\partial r} \left[\frac{\rho r^2}{10(1 + s h_n)} \left\{ \begin{aligned} & s \left(h_n^4 + \frac{2c^2}{3} h_n^2 + \frac{c^4}{33} \right) (3\Omega_u^2 + 4\Omega_u\Omega_l + 3\Omega_l^2) \\ & + 2 \left(h_n^3 + \frac{c^2}{3} h_n \right) (4\Omega_u^2 + 7\Omega_u\Omega_l + 9\Omega_l^2) \end{aligned} \right\} \right] \\ & \quad - 12\eta \dot{h}_0 + 24\rho\phi_r H^* \Omega_l^2. \end{aligned} \quad (5.17)$$

Circumferential Roughness Pattern

In this model, the roughness is assumed to have the form of long, narrow ridges and valleys running in θ -direction. The film thickness in this case assumes the form

$$h = h_n + h_s(r, \xi). \quad (5.18)$$

Taking expected values of both sides of equation (5.12), yields (referring [26])

$$\begin{aligned} & \frac{1}{r} \frac{\partial}{\partial r} \left[\left\{ 12\phi_r H^* + \frac{4[E(h^{-3})]^{-1} + s[E(h^{-4})]^{-1}}{1 + sE(h)} \right\} r \frac{\partial}{\partial r} \left\{ E(p) - \frac{1}{2} \mu_0 \bar{\mu} H^2 \right\} \right] \\ &= \frac{1}{r} \frac{\partial}{\partial r} \left[\frac{\rho r^2}{10\{1 + sE(h)\}} \left\{ s[E(h^{-4})]^{-1} (3\Omega_u^2 + 4\Omega_u \Omega_l + 3\Omega_l^2) \right. \right. \\ & \quad \left. \left. + 2[E(h^{-3})]^{-1} (4\Omega_u^2 + 7\Omega_u \Omega_l + 9\Omega_l^2) \right\} \right] \\ & \quad - 12\eta \dot{h}_0 + 24\rho\phi_r H^* \Omega_l^2, \end{aligned} \quad (5.19)$$

where $E(*)$ is the expectancy operator defined by equation (5.16).

Using equation (5.16) stochastic Reynolds equation in this case can be obtained as

$$\begin{aligned} & \frac{1}{r} \frac{\partial}{\partial r} \left[\left\{ 12\phi_r H^* + \frac{4 \left(h_n^3 - \frac{2c^2}{3} h_n \right) + s \left[h_n^4 - \frac{70c^2}{63} h_n^2 + \left(\frac{70}{63} \right)^2 c^4 \right]}{1 + sh_n} \right\} r \frac{\partial}{\partial r} \left\{ E(p) - \frac{1}{2} \mu_0 \bar{\mu} H^2 \right\} \right] \\ &= \frac{1}{r} \frac{\partial}{\partial r} \left[\frac{\rho r^2}{10(1 + sh_n)} \left\{ s \left[h_n^4 - \frac{70c^2}{63} h_n^2 + \left(\frac{70}{63} \right)^2 c^4 \right] (3\Omega_u^2 + 4\Omega_u \Omega_l + 3\Omega_l^2) \right. \right. \\ & \quad \left. \left. + 2 \left(h_n^3 - \frac{2c^2}{3} h_n \right) (4\Omega_u^2 + 7\Omega_u \Omega_l + 9\Omega_l^2) \right\} \right] \\ & \quad - 12\eta \dot{h}_0 + 24\rho\phi_r H^* \Omega_l^2. \end{aligned} \quad (5.20)$$

In order to form a single equation for both the roughness patterns, substituting

$$f(h_n, c) = \begin{cases} h_n^3 + \frac{c^2}{3} h_n & (\text{radial roughness}) \\ h_n^3 - \frac{2c^2}{3} h_n & (\text{circumferential roughness}) \end{cases}$$

$$g(h_n, c) = \begin{cases} h_n^4 + \frac{2c^2}{3} h_n^2 + \frac{c^4}{33} & (\text{radial roughness}) \\ h_n^4 - \frac{70c^2}{63} h_n^2 + \left(\frac{70}{63}\right)^2 c^4 & (\text{circumferential roughness}) \end{cases}$$

equations (5.17) and (5.20), implies

$$\begin{aligned} & \frac{1}{r} \frac{\partial}{\partial r} \left[\left\{ 12 \phi_r H^* + \frac{4f(h_n, c) + s g(h_n, c)}{1 + sh_n} \right\} r \frac{\partial}{\partial r} \left\{ E(p) - \frac{1}{2} \mu_0 \bar{\mu} H^2 \right\} \right] \\ & = \frac{1}{r} \frac{\partial}{\partial r} \left[\frac{\rho r^2}{10(1 + sh_n)} \left\{ s g(h_n, c)(3\Omega_u^2 + 4\Omega_u \Omega_l + 3\Omega_l^2) \right. \right. \\ & \quad \left. \left. + 2f(h_n, c)(4\Omega_u^2 + 7\Omega_u \Omega_l + 9\Omega_l^2) \right\} \right] \\ & \quad - 12\eta \dot{h}_0 + 24\rho \phi_r H^* \Omega_l^2, \end{aligned} \tag{5.21}$$

which is the required Reynolds equation of the present study.

Introducing dimensionless quantities as follows.

$$\begin{aligned} R &= \frac{r}{a}, \quad C = \frac{c}{h_0}, \quad \bar{h}_n = \frac{h_n}{h_0}, \quad \bar{p} = -\frac{E(p)h_0^3}{a^2 \eta \dot{h}_0}, \\ \psi_r &= \frac{\phi_r H^*}{h_0^3}, \quad \bar{s} = sh_0, \quad S = -\frac{\rho \Omega_u^2 h_0^3}{\eta \dot{h}_0}, \quad \Omega_f = \frac{\Omega_l}{\Omega_u}, \quad \mu^* = -\frac{K \mu_0 \bar{\mu} h_0^3}{\eta \dot{h}_0} \end{aligned} \tag{5.22}$$

Equation (5.21) becomes

$$\frac{1}{R} \frac{\partial}{\partial R} \left[RF \frac{\partial}{\partial R} \left\{ \bar{p} - \frac{1}{2} \mu^* R^2 (1 - R) \right\} \right] = \frac{1}{R} \frac{\partial}{\partial R} (GR), \tag{5.23}$$

where

$$F = 12 \psi_r + \frac{4F(\bar{h}_n, C) + \bar{s} G(\bar{h}_n, C)}{1 + \bar{s} \bar{h}_n}, \quad (5.24)$$

$$G = \frac{SR}{1 + \bar{s} \bar{h}_n} \left[\frac{\bar{s} G(\bar{h}_n, C)}{10} (3 + 4\Omega_f + 3\Omega_f^2) + \frac{F(\bar{h}_n, C)}{5} (4 + 7\Omega_f + 9\Omega_f^2) \right] + 6R + 12SR\psi_r\Omega_f^2, \quad (5.25)$$

$$F(\bar{h}_n, C) = \begin{cases} \bar{h}_n^3 + \frac{C^2}{3} \bar{h}_n & (\text{radial roughness}) \\ \bar{h}_n^3 - \frac{2C^2}{3} \bar{h}_n & (\text{circumferential roughness}) \end{cases}$$

$$G(\bar{h}_n, C) = \begin{cases} \bar{h}_n^4 + \frac{2C^2}{3} \bar{h}_n^2 + \frac{C^4}{33} & (\text{radial roughness}) \\ \bar{h}_n^4 - \frac{70C^2}{63} \bar{h}_n^2 + \left(\frac{70}{63}\right)^2 C^4 & (\text{circumferential roughness}) \end{cases}$$

$$f(h_n, c) = h_0^3 F(\bar{h}_n, C) \text{ g}$$

$$g(h_n, c) = h_0^4 G(\bar{h}_n, C)$$

$$H^2 = KR^2 a^2 (1 - R)$$

5.3 Solution

Solving equation (5.23) for the following relevant boundary conditions [21]

$$\bar{p} = 0 \quad \text{when } R=1, \quad \frac{\partial \bar{p}}{\partial R} = 0 \quad \text{when } R=0,$$

the dimensionless film pressure can be obtained as

$$\bar{p} = \frac{1}{2} \mu^* R^2 (1 - R) - \int_R^1 \frac{G}{F} dR. \quad (5.26)$$

From the definition of the mean load-carrying capacity

$$E(W) = 2\pi \int_0^a E(p) r dr = -\frac{2\pi a^4 \eta \dot{h}_0}{h_0^3} \int_0^1 \bar{p} R dR,$$

the dimensionless load-carrying capacity can be obtained as

$$\bar{W} = \frac{E(W) h_0^3}{2\pi a^4 \eta \dot{h}_0} = -\int_0^1 \bar{p} R dR = -\frac{\mu^*}{40} + \frac{1}{2} \int_0^1 \frac{G}{F} R^2 dR, \quad (5.27)$$

where F and G are given by equations (5.24) and (5.25), respectively.

5.4 Results and Discussion

The results of dimensionless load-carrying capacity \bar{W} for different bearing designs (exponential, secant, mirror image of secant and parallel) are calculated from equation (5.27) for the following values of the different parameters using Simpson's rule with step size 0.1. Here, the values of the different parameters remains fixed during calculations unless and until the study is made w.r.t. the variation of the particular parameter.

$$\begin{aligned} a &= 0.075 \text{ (m)}, h_0 = 5.0 \times 10^{-5} \text{ (m)}, \eta_r = 0.25, \\ \rho &= 1390 \text{ (Ns}^2\text{m}^{-4}\text{)}, \eta = 0.0327 \text{ (Nsm}^{-2}\text{)}, \bar{\mu} = 0.05, \bar{\beta} = 0.6, \\ \mu_0 &= 4\pi \times 10^{-7} \text{ (NA}^{-2}\text{)}, \Omega_u = 30\pi \text{ (rad.s}^{-1}\text{)}, \Omega_l = 70\pi \text{ (rad.s}^{-1}\text{)}, \\ K &= 10^9 / 0.83, \dot{h}_0 = 0.005 \text{ (ms}^{-1}\text{)}, H^* = 5.0 \times 10^{-5} \text{ (m)} \end{aligned}$$

The shapes of the different bearing designs due to the variation in shape of the upper disc are given by the following dimensionless forms. It should be noted here that due to different bearing designs the film thickness h also takes different forms.

(1) For exponentially curved upper disc

$$\bar{h}_n = e^{-\bar{\beta} R^2}; \bar{\beta} = \beta a^2 \quad 0 \leq R \leq 1$$

(2) For secant curved upper disc

$$\bar{h}_n = \sec(\bar{\beta} R^2); \bar{\beta} = \beta a^2 \quad 0 \leq R \leq 1$$

(3) For mirror image of secant curved upper disc

$$\bar{h}_n = 2 - \sec(\bar{\beta} R^2); \bar{\beta} = \beta a^2 \quad 0 \leq R \leq 1$$

(4) For parallel upper disc

$$\bar{h}_n = 1; \quad 0 \leq R \leq 1$$

where β is the curvature of the upper discs.

The strength of the magnetic field considered throughout the study is of order 3; that is, $O(H) \approx 3$.

Figures 5.2-5.4 shows the graphical presentation of the calculated results of \bar{W} .

Figure 5.2 shows the variation in \bar{W} for all designs (exponential, secant, mirror image of secant and parallel (flat)) squeeze-film-bearings as a function of dimensionless circumferential roughness parameter C considering dimensionless radial permeability parameter $\psi_r = 0.00002$. It is observed that \bar{W} increases moderately with the increase of C . Moreover, \bar{W} is more in the case of exponential shape. The following inequality of \bar{W} is obtained for all designs.

$$\bar{W}_e > \bar{W}_{is} > \bar{W}_p > \bar{W}_s,$$

where \bar{W}_e , \bar{W}_{is} , \bar{W}_p , \bar{W}_s are respectively dimensionless load-carrying capacity for exponential, mirror image of secant, parallel and secant squeeze-film-bearings.

Figure 5.3 shows the variation in \bar{W} as a function of dimensionless radial permeability parameter ψ_r , considering dimensionless circumferential roughness

parameter $C = 0.04$. The case of exponential squeeze-film-bearing is studied. It is observed that \bar{W} decreases with the increase of ψ_r . This happens because due to higher permeability, the more readily does fluid flow out through the porous material. This reason can also be justified by the following references.

According to Sparrow *et. al.* [27], when porous matrix is attached with the solid disc, the pressure in the porous medium provides a path for the fluid to come out to the environment from the bearing, which leads to decrease in resistance of flow in r – direction and as a consequence the \bar{W} is reduced. This behaviour of decreasing \bar{W} with the insertion of porous matrix also agrees with the conclusions of Prakash and Tiwari [28] while discussing the problem of squeeze-film of rough porous rectangular discs theoretically (which was studied experimentally by Wu [29]).

Figure 5.4 shows the variation in \bar{W} as a function of dimensionless roughness parameter C , which includes case of radial and circumferential roughness patterns, considering $\psi_r = 0.00002$. The case of exponential squeeze-film-bearing is studied. It is observed that with the increase of circumferential roughness pattern, \bar{W} increases significantly whereas with the increase of radial roughness pattern, \bar{W} decreases. This opposite nature of \bar{W} w.r.t. both the roughness patterns may be because of the following reason.

In the present case porous matrix is attached with the lower disc and in addition to above three references [27-29], circumferential and radial roughness patterns of the porous matrix is also considered. Therefore, roughness patterns also effect on \bar{W} . For

circumferential roughness pattern, structure of surface having deviation (from nominal level) w.r.t. r , which leads the possibility of the retention of the fluid in the gaps and so some resistance of flow in r – direction appears. Due to this reason, the fluid come out to the environment becomes comparatively less and which results in the increase of \bar{W} as compared to radial pattern. In radial pattern, the situation is different because the structure of surface having deviation w.r.t. θ which does not lead the retention of the fluid in r –direction.

Figure 5.5 shows the variation in \bar{W} as a function of dimensionless radial permeability parameter ψ_r , considering case of radial and circumferential roughness patterns for $C = 0.04$. The case of exponential squeeze-film-bearing is studied. It is again observed that \bar{W} is more in the case of circumferential roughness pattern.

5.5 Conclusions

Based on FF flow model by R.E. Rosensweig, equation of continuity for film as well as porous region and roughness effect by Christensen's stochastic theory, modified Reynolds equation for circular squeeze-film-bearing, formed between upper solid impermeable disc and lower porous-rough disc, is derived. Two roughness patterns, radial and circumferential, on the porous surface are also included in the study. Moreover, the porous-rough surface is considered because of obtaining advantage of self-lubricating property of the bearing design system. Here, the FF is controlled by radially VMF because of obtaining advantage of generating maximum field at the required active contact zone. Moreover, for this FF flow model uniform magnetic field

does not have any effect on the performance of the bearing characteristics. In the porous region validity of the Darcy's is assumed. The effects of permeability and surface roughness on dimensionless load-carrying capacity are studied and compared for different bearing design systems (exponential, secant, mirror image of secant and parallel (flat)). The purpose of considering the present problem is lies in the observation that most of studies on different designs of squeeze-films (sphere-plate, cylindrical-disc, two-parallel plates, etc.) reduce to the present case. The following conclusions can be made from results and discussion.

- (1) \bar{W} is significantly more for exponential squeeze-film-bearing as compared to other shapes. The following comparison of load-carrying capacity is obtained for all designs.

$$\bar{W}_e > \bar{W}_{is} > \bar{W}_p > \bar{W}_s .$$

For exponential squeeze-film-bearing design

- (2) \bar{W} decreases with the increase of ψ_r .
- (3) \bar{W} increases significantly with the increase of circumferential roughness pattern, whereas decreases with the increase of radial roughness pattern.

The study indicates the favour of designing circumferentially rough, porous exponential shape squeeze-film bearing with smaller values of radial permeability parameter.

5.6 Figures

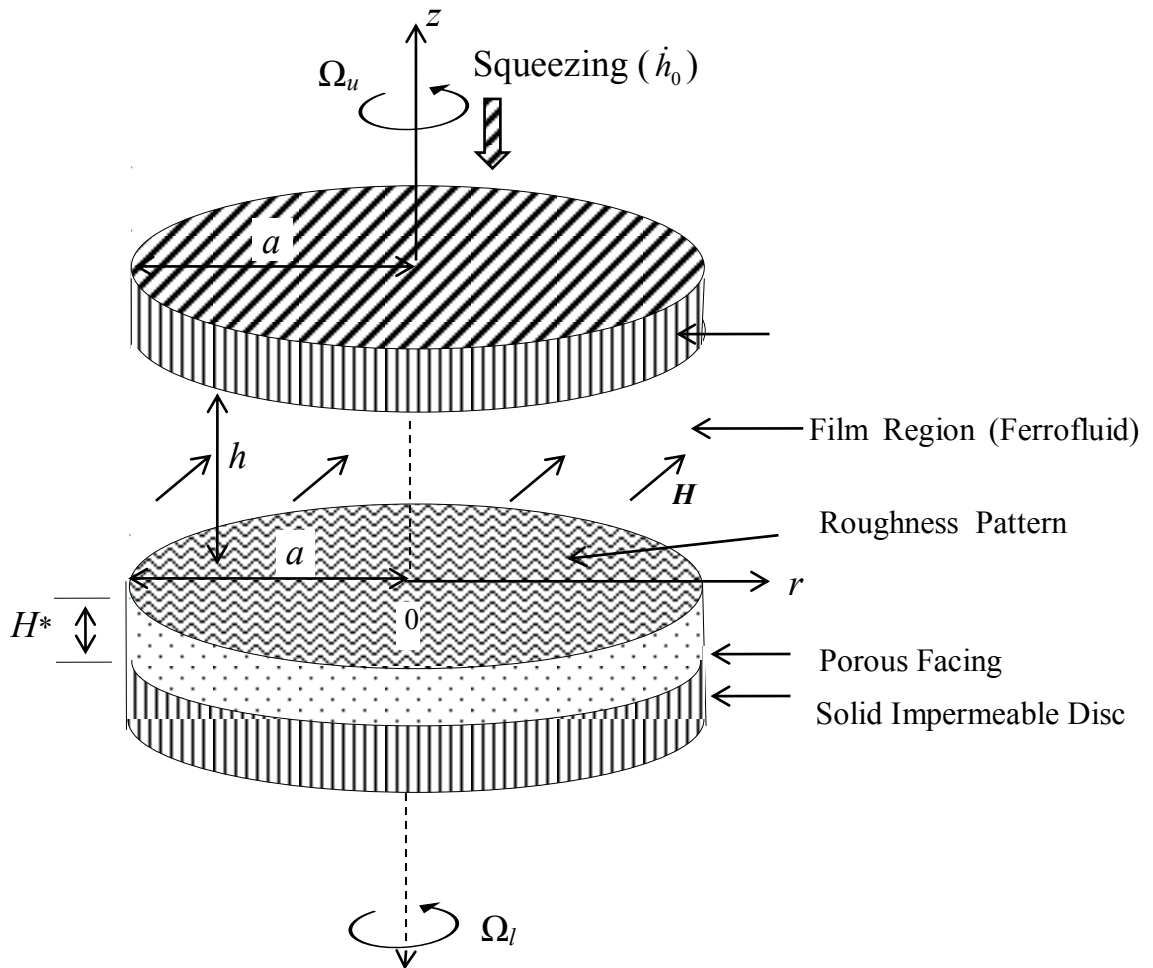


Figure 5.1

Squeeze-film geometry between upper solid impermeable disc and lower porous-rough disc.

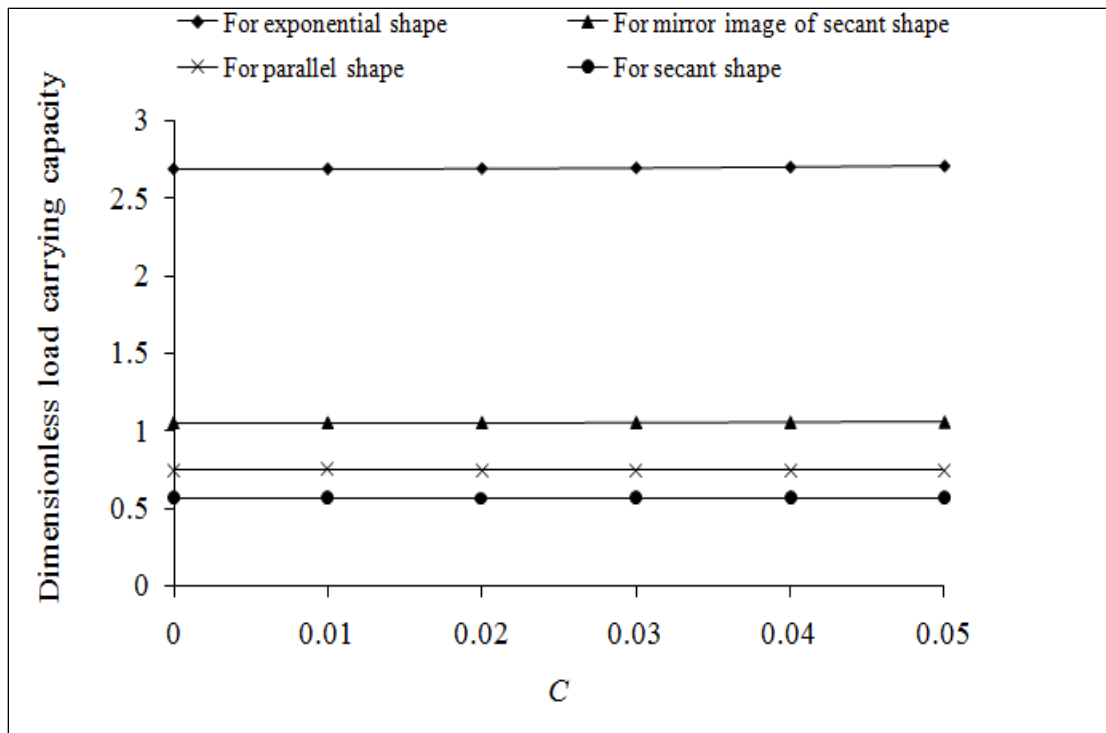


Figure 5.2

Variation in dimensionless load-carrying capacity \bar{W} for different values of dimensionless circumferential roughness parameter C considering

$$\psi_r = 0.00002$$

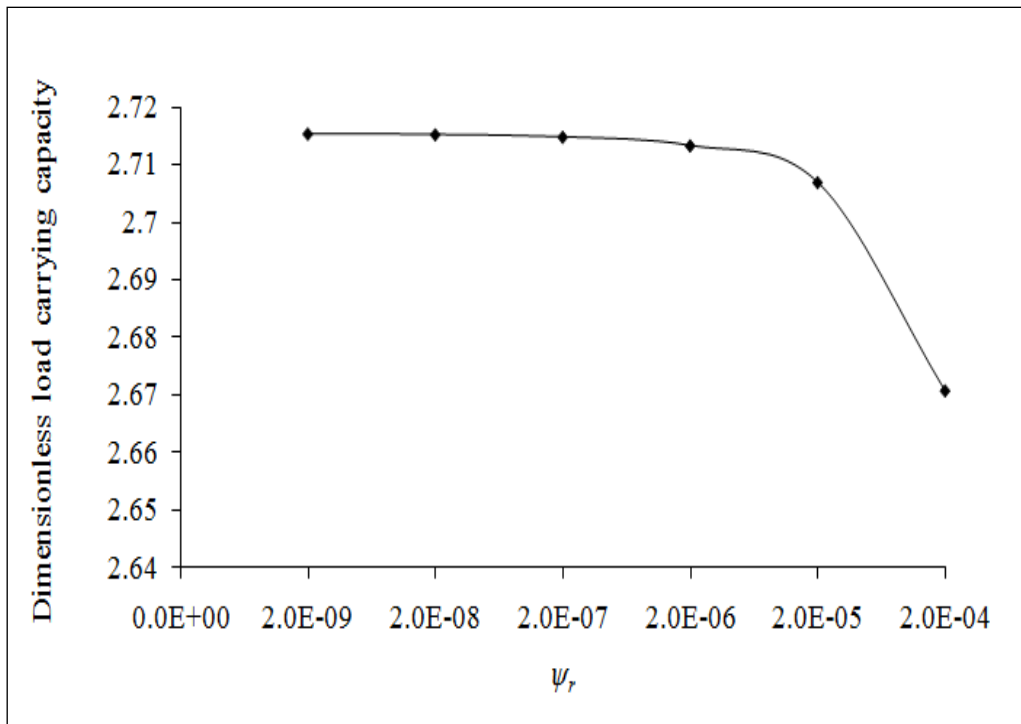


Figure 5.3

Variation in dimensionless load-carrying capacity \bar{W} for different values of dimensionless radial permeability parameter ψ_r , considering dimensionless circumferential roughness parameter $C = 0.04$

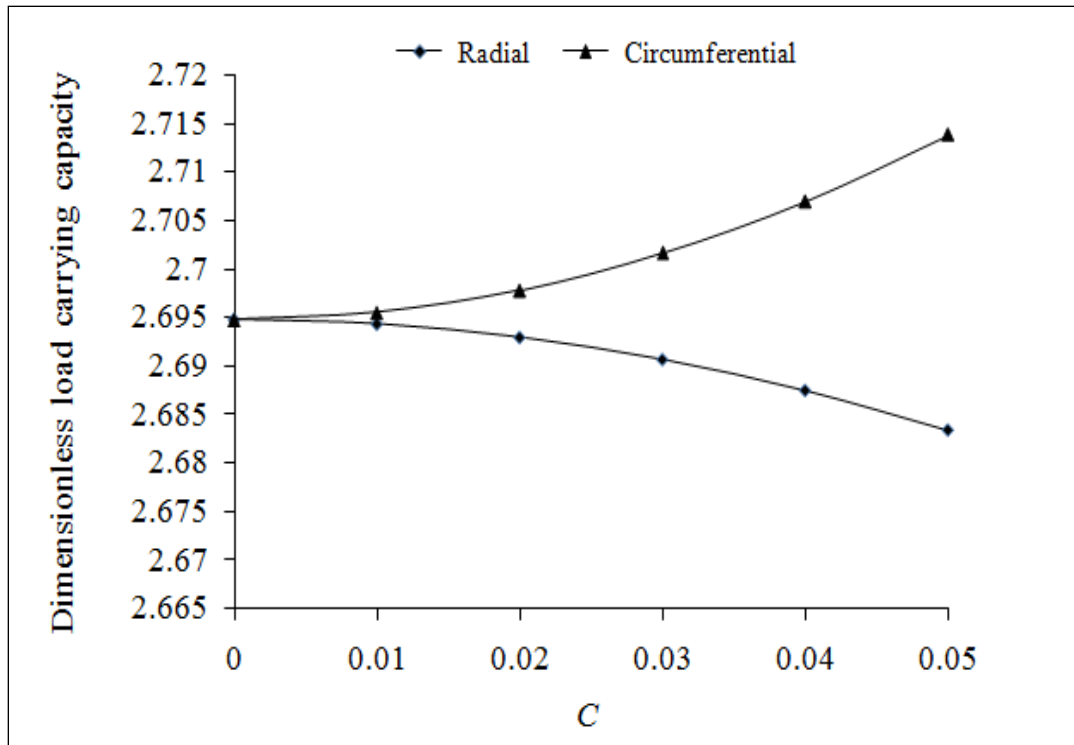


Figure 5.4

Variation in dimensionless load-carrying capacity \bar{W} for different values of dimensionless roughness parameter C considering $\psi_r = 0.00002$

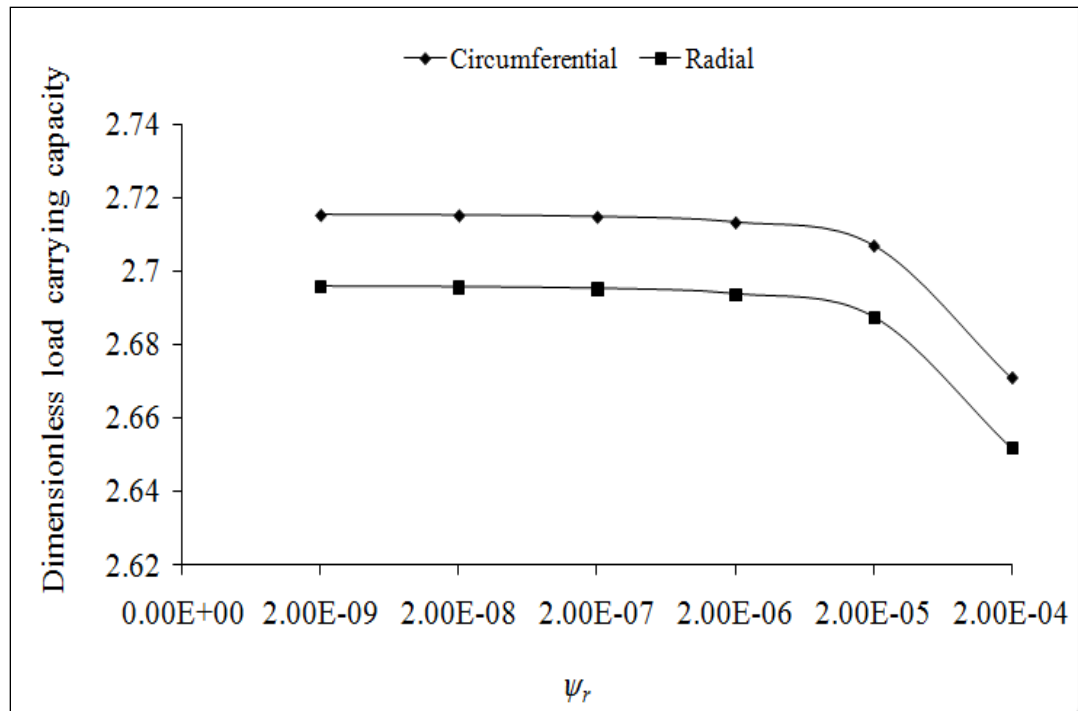


Figure 5.5

Variation in dimensionless load-carrying capacity \bar{W} for different values of dimensionless radial permeability parameter ψ_r , considering

$$C = 0.04$$

5.7 References

- [1] R.E. Rosensweig, *Ferrohydrodynamics*, New York. NY: *Cambridge University Press* (1985).
- [2] K. Raj and R. Moskowitz, Commercial applications of ferrofluids, *Journal of Magnetism and Magnetic Materials* 85 (1990) 233-245.
- [3] I. Torres-Diaz and C. Rinaldi, Recent progress in ferrofluids research: novel applications of magnetically controllable and tunable fluids, *Soft Matter* 10 (2014) 8584-8602.
- [4] P.R.K. Murti, Squeeze-film behaviour in porous circular disks, *Transactions of the ASME* 96 (1974) 206-209.
- [5] L.L. Ting, Engagement behaviour of lubricated porous annular disks, part I: squeeze-film phase –surface roughness and elastic deformation effects, *Wear* 34 (1975) 159-182.
- [6] J. Prakash and K. Tonder, Roughness effects in circular squeeze- plates, *ASLE Transactions* 20 (1977) 257-263.
- [7] P.D.S. Verma, Magnetic fluid-based squeeze-film, *International journal of Engineering Science* 24 (1986) 395-401.
- [8] M.V. Bhat and G.M. Deheri, Magnetic-fluid-based squeeze-film in curved porous circular discs, *Journal of Magnetism and Magnetic Materials* 127 (1993) 159-162.
- [9] A.A. Elsharkawy and M.M. Nassar, Hydrodynamic lubrication of squeeze- film porous bearings, *Acta Mechanica* 118 (1996) 121-134.
- [10] R.C. Shah, S.R. Tripathi and M.V.Bhat, Magnetic fluid based squeeze-

- film between porous annular curved plates with the effect of rotational inertia, *Pramana-Journal of Physics* 58 (2002) 545-550.
- [11] R. Usha and P. Vimala, Squeeze-film force using an elliptical velocity profile, *ASME Journal of Applied Mechanics* 70 (2003) 137-142.
- [12] R.C. Shah and M.V. Bhat, Anisotropic permeable porous facing and slip velocity on squeeze-film in an axially undefined journal bearing with ferrofluid lubricant, *Journal of Magnetism and Magnetic Materials* 279 (2004) 224-230.
- [13] M.J. Jaffer, Squeeze-films between a rigid cylinder and an elastic layer bonded to a rigid foundation, *Tribology International* 40 (2007) 567-572.
- [14] N.M. Bujurke, D.P. Basti and R.B. Kudenatti, Surface roughness effects on squeeze-film behaviour in porous circular disks with couple stress fluid, *Transp Porous Med* 71 (2008) 185-197.
- [15] M. Rajashekar and B. Kashinath, Effect of surface roughness on MHD couple stress squeeze-film characteristics between a sphere and a porous plane surface, *Advances in Tribology* (2012) Article ID 935690: 10 pages.
- [16] S. Kesavan, A.J. Chamkha and S.K. Narayanan, Magnetohydrodynamic (MHD) squeeze-film characteristics between finite porous parallel rectangular plates with surface roughness, *International Journal of Numerical Methods for Heat & Fluid Flow* 24 (2014) 1595-1609.

- [17] A. Walicka, E. Walicki, P. Jurczak and J. Falicki, Porous squeeze-film bearing with rough surfaces lubricated by a bingham fluid, *International Journal of Applied Mechanics and Engineering* 19 (2014) 795-808.
- [18] S.T. Fathima, N.B. Naduvinamani, S.H. Marulappa and H. Bannihalli, A study on the performance of hydromagnetic squeeze-film between anisotropic porous rectangular plates with couplestress fluids, *Tribology Online* 9 (2014) 1-9.
- [19] J.R. Lin, L.J. Liang, M.C. Lin and S.T. Hu, Effects of circumferential and radial rough surfaces in a non-Newtonian magnetic fluid lubricated squeeze-film, *Applied Mathematical modeling* 39 (2015) 6743-6750.
- [20] R.C. Shah and R.C. Kataria, On the squeeze-film characteristics between a sphere and a flat porous plate using Ferrofluid, *Applied Mathematical Modelling* 40 (2016) 2473-2484.
- [21] R.C. Shah and D.A. Patel, On the ferrofluid lubricated squeeze-film characteristics between a rotating sphere and a radially rough plate, *Meccanica* 51 (2016) 1973-1984.
- [22] R.C. Shah, N.I. Patel and R.C. Kataria, Some porous squeeze-film bearings using ferrofluid lubricant: A review with contributions, *Journal of Engineering Tribology* 230 (2016) 1157-1171.
- [23] R.C. Shah and M.V. Bhat, Ferrofluid lubrication of a parallel plate squeeze-film bearing, *Theoretical and Applied Mechanics* 30 (2003) 221-240.

- [24] K.H. Vora and M.V. Bhat, The load capacity of a squeeze-film between curved porous rotating circular plates, *Wear* 65 (1980) 39-46.
- [25] H. Christensen, Stochastic models for hydrodynamic lubrication of rough surfaces, *Proc Instn Mech Engrs* 184 (1969) 1013.
- [26] J. Prakash and K. Tiwari, Effect of surface roughness on the squeeze-film between rotating porous annular discs with arbitrary porous wall thickness, *International Journal of Mechanical Science* 27 (1985) 135-144.
- [27] E.M. Sparrow, G.S. Beavers and I.T. Hwang, Effect of velocity slip on porous-walled squeeze films, *Journal of Lubrication Technology* 94 (1972) 260-264.
- [28] J. Prakash and K. Tiwari, Lubrication of a porous bearing with surface corrugations, *Journal of Lubrication Technology* 104 (1982) 127-134.
- [29] H. Wu, A review of porous squeeze-films, *Wear* 47 (1978) 371-385.